JOURNAL OF APPLIED PHYSICS 118, 115706 (2015)

Observation of silicon self-diffusion enhanced by the strain originated from end-of-range defects using isotope multilayers

Taiga Isoda, Masashi Uematsu, and Kohei M. Itoh[a)]
School of Fundamental Science and Technology, Keio University, 3-14-1 Hiyoshi, Kohoku-ku, Yokohama 223-8522, Japan

(Received 24 July 2015; accepted 8 September 2015; published online 18 September 2015)

Si self-diffusion in the presence of end-of-range (EOR) defects is investigated using $^{nat}Si/^{28}Si$ isotope multilayers. The isotope multilayers were amorphized by Ge ion implantation, and then annealed at 800–950 °C. The behavior of Si self-interstitials is investigated through the ^{30}Si self-diffusion. The experimental ^{30}Si profiles show further enhancement of Si self-diffusion at the EOR defect region, in addition to the transient enhanced diffusion via excess Si self-interstitials by EOR defects. To explain this additional enhanced diffusion, we propose a model which takes into account enhanced diffusion by tensile strain originated from EOR defects. The calculation results based on this model have well reproduced the experimental ^{30}Si profiles. © *2015 AIP Publishing LLC*.
[http://dx.doi.org/10.1063/1.4931421]

I. INTRODUCTION

Ultra-shallow junction formation is one of the most crucial issues for continuous scaling down of Si device processing. The most established method to form ultra-shallow junction is pre-amorphizing implants (PAIs), where non-dopant ions, usually Ge, are implanted with high dose prior to dopant implantation.[1–3] The main advantage of using PAI is the reduction of dopant channeling. Furthermore, the damage in the amorphized region is almost totally eliminated through solid phase epitaxial regrowth during post-implant annealing; only the damage that exists in the non-amorphized tail beyond the amorphous/crystalline (a/c) interface remains.[4] However, the PAI process induces the formation of end-of-range (EOR) defects beneath the a/c interface.[5] EOR defects are interstitial-type dislocation loops and become a source of transient enhanced diffusion (TED).[6–9] Upon annealing, EOR defects grow in size and reduce their density while the total number of Si self-interstitials stored in the loops remains constant. This coarsening process is Ostwald ripening and reduces the efficiency of EOR defects as a source of Si self-interstitials.[1,6] In order to investigate the time-dependent behavior of Si self-interstitials in the presence of EOR defects, boron (B) atoms have been used as markers[4,9–11] because B diffusion in Si is governed by the interstitial mechanism.[12]

There is another possibility of diffusion enhancement by EOR defects. Experimental results of X-ray analysis show the presence of tensile strain at EOR defect regions.[13–15] This tensile strain at EOR defects can enhance B diffusion because theoretical calculations found that tensile strain enhances interstitial-mediated diffusion.[16] To the best of our knowledge, however, there have been no reports that show enhanced B diffusion at EOR defect regions although B diffusion in the presence of EOR defects has been extensively studied. This is probably due to B trapping at EOR defects,[17] which is likely to mask the enhanced B diffusion by tensile strain. Note that dopant trapping (or segregation) has been reported for indium,[18] phosphorus,[15] and arsenic,[19] which diffuse via the interstitial mechanism, and hence, these dopants may be also enhanced at EOR defects but masked by the trapping.

In this study, in order to avoid such disturbance from dopant trapping, we investigate Si self-diffusion using isotope Si multilayers that are amorphized by Ge implantation. The behavior of Si self-interstitials is directly observed through Si self-diffusion.[20–23] We observe further enhanced Si self-diffusion at the EOR defect region, in addition to the TED by EOR defects. We show that this enhancement can be explained by tensile strain induced by EOR defects.

II. EXPERIMENTS

Isotopically enriched ^{28}Si and natural Si (^{28}Si: 92.2%, ^{29}Si: 4.7%, and ^{30}Si: 3.1%) multilayers were grown by solid source molecular beam epitaxy on a (100)-oriented B-doped Czochralski Si wafer with a resistivity of 1–20 Ω cm.[20,21,24] A ^{nat}Si buffer layer of ∼150-nm-thick was grown prior to the growth of the isotope multilayers that are composed of the alternating layers of ^{28}Si and ^{nat}Si. ^{nat}Si layers have the natural abundance with 3.1% of ^{30}Si, whereas ^{28}Si layers are depleted of ^{30}Si. Si self-diffusion is evaluated by observing the change of ^{30}Si depth profiles after annealing. The isotope multilayers were amorphized by $^{74}Ge^{+}$ ion implantation with an energy of 150 keV and a dose of $2 \times 10^{15}\,cm^{-2}$ at room temperature. The isotope multilayers were annealed at 800–950 °C in a resistance furnace under an Ar (99.99%) atmosphere. The depth profiles of ^{30}Si and ^{74}Ge were measured by secondary ion mass spectrometry (SIMS). Primary ions used in SIMS were O^{2+} with an energy of 1.0 keV for ^{30}Si, and Cs^{+} with 3.0 keV for ^{74}Ge.

III. RESULTS

Figure 1 shows the depth profile of ^{30}Si in the Si isotope multilayers before Ge implantation (as-grown) measured by

a)Electronic mail: kitoh@appi.keio.ac.jp

 © 2015 AIP Publishing LLC

[This article is copyrighted as indicated in the article. Reuse of AIP content is subject to the terms at: http://scitation.aip.org/termsconditions. Downloaded to] IP: 131.113.64.57 On: Tue, 06 Oct 2015 08:51:35

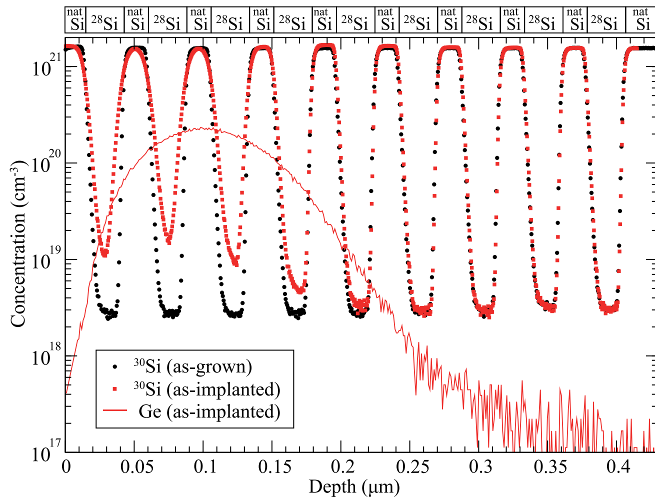

FIG. 1. SIMS profiles of ^{30}Si in the ^{nat}Si/^{28}Si isotope multilayers before (as-grown) and after (as-implanted) Ge implantation at 150 keV, $2 \times 10^{15}\,\mathrm{cm}^{-2}$. The implanted Ge depth profile is also presented. Symbols and solid lines represent the profiles of ^{30}Si and Ge, respectively. The structure of isotope multilayers is schematically shown at the top of the figure.

SIMS. The ^{nat}Si/^{28}Si periodic structure is schematically shown at the top of the figure. The actual interfaces between ^{nat}Si and ^{28}Si layers are abrupt (the degree of intermixing is only two atomic layers)[20,21,24] and the smearing of the ^{nat}Si and ^{28}Si profiles is due to the SIMS artifact (knock-on mixing, etc.). The periodic profile was perturbed after Ge implantation (as-implanted), as shown in Fig. 1, where the Ge depth profile is also presented. This perturbation of the profile is due to Si displacement induced by Ge implantation.[25] Figure 2(a) shows the image of cross-sectional transmission electron microscopy (XTEM) of the as-implanted sample. Due to the implantation, amorphization occurred between the surface and 175 nm in depth, while the deeper region (x > 175 nm) remained single-crystalline. After annealing, the samples observed by XTEM show EOR defects just beneath the former a/c interface, i.e., at the depth of 175–225 nm [Fig. 2(b)]. Figure 3 shows the depth profiles of ^{30}Si in samples annealed at (a) 800 °C, (b) 900 °C, and (c) 950 °C. The ^{30}Si profiles showed that Si self-diffusion was enhanced by EOR defects and significantly larger than the thermal equilibrium Si self-diffusion, which we have investigated using similar isotope heterostructures.[20] In addition to this enhancement, further enhanced diffusion is observed at the fifth ^{28}Si layer of multilayers in all annealing conditions. Note that the region where this additional enhancement is observed well coincides with the position of EOR defects shown in Fig. 2(b). We will describe below that it can be the enhanced diffusion due to tensile strain induced by EOR defects, which we have predicted in the introduction.

IV. DISCUSSION

A. TED via excess Si self-interstitials by EOR defects

In order to investigate the diffusion enhancement by tensile strain, we first fit the ^{30}Si profiles based on our TED model[8] that does not take the strain enhancement into account. Si self-diffusion is governed by interstitial and vacancy mechanisms[20,22] and is described by the following reactions:

$$^{30}I \leftrightarrow {}^{30}\mathrm{Si}_S + I, \qquad (1)$$

$$^{30}V \leftrightarrow {}^{30}\mathrm{Si}_S + V, \qquad (2)$$

$$I + V \leftrightarrow \emptyset. \qquad (3)$$

Here, $^{30}\mathrm{Si}_S$ denotes substitutional ^{30}Si. I and ^{30}I denote the Si self-interstitial of ^{28}Si (matrix) and ^{30}Si, respectively, and V represents the vacancy of ^{28}Si (matrix). ^{30}V denotes the configuration in which ^{30}Si becomes mobile through site exchange with V, in a similar manner to a dopant-vacancy pair, assuming that there is no binding between ^{30}Si and V. We have used the same type of configuration to simulate germanium (Ge) self-diffusion.[26] Reactions (1) and (2) describe

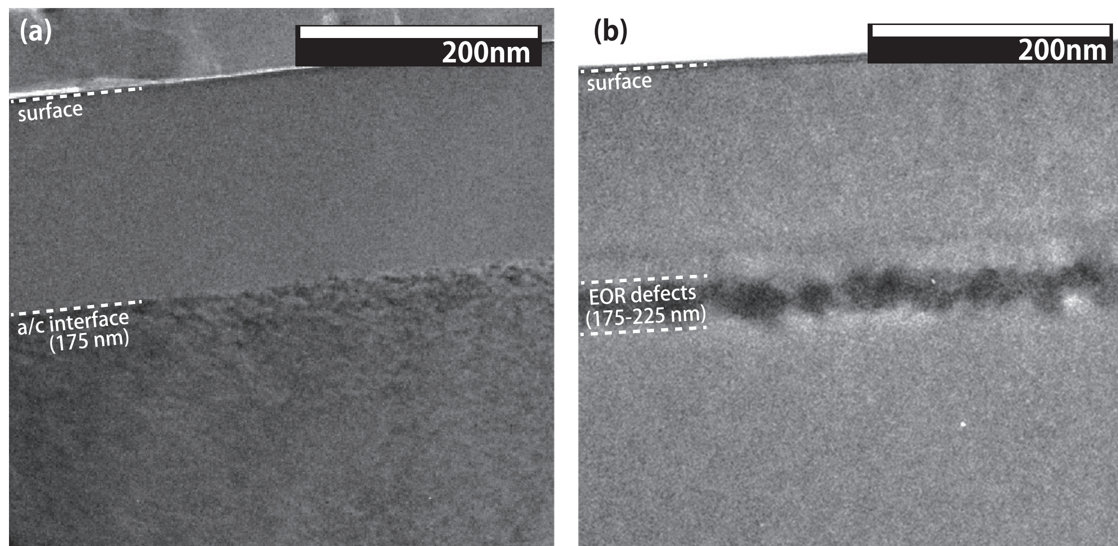

FIG. 2. Bright-field XTEM images of Ge implanted samples. (a) The as-implanted sample, where amorphization occurred between the surface and 175 nm in depth. (b) The sample annealed at 950 °C for 30 s, where EOR defects were formed just beneath the former a/c interface at the depth of 175–225 nm.

[This article is copyrighted as indicated in the article. Reuse of AIP content is subject to the terms at: http://scitation.aip.org/termsconditions. Downloaded to] IP: 131.113.64.57 On: Tue, 06 Oct 2015 08:51:35

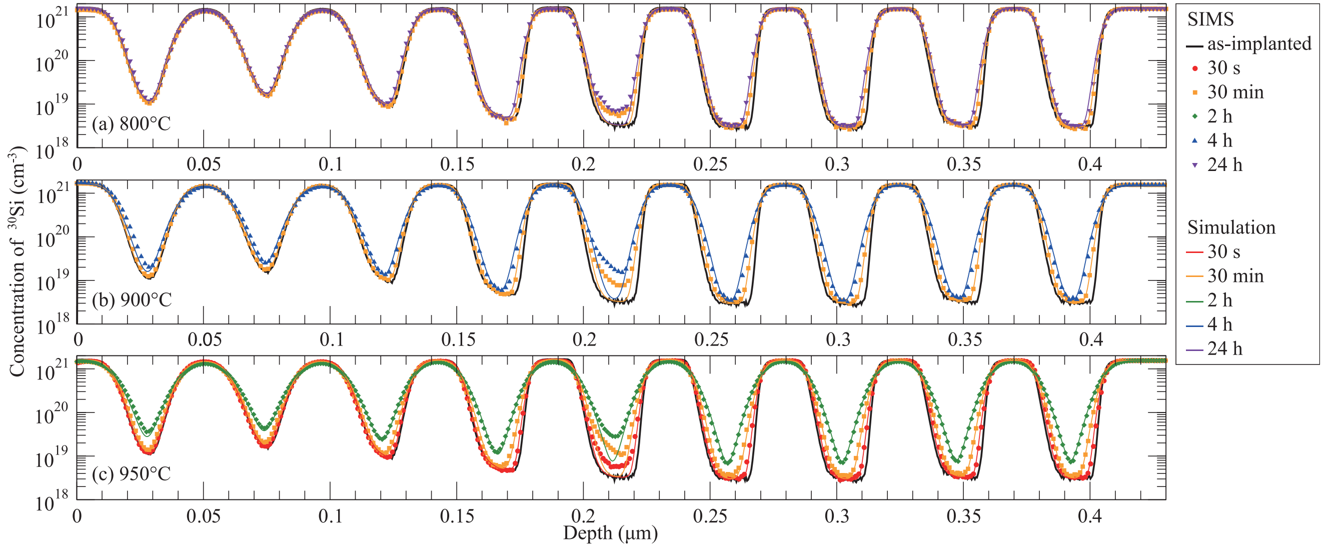

FIG. 3. SIMS and calculated profiles of ^{30}Si with 150 keV, $2 \times 10^{15}\,\mathrm{cm}^{-2}$ Ge implantation and annealing at (a) 800 °C for 30 min and 24 h, (b) 900 °C for 30 min and 4 h, and (c) 950 °C for 30 s, 30 min, and 2 h. Symbols and solid lines represent SIMS and calculated profiles, respectively. The SIMS profile before annealing (as-implanted) is also shown by a thick solid line. The calculation is based on the TED model that does not take into account diffusion enhancement by strain at EOR defects.

interstitial and vacancy mechanisms, respectively, and reaction (3) represents I-V generation-recombination (g-r). The vacancy contribution to Si self-diffusion is taken into account, although it is much smaller than the interstitial contribution during TED, because the vacancy contribution cannot be neglected when the diffusion is closer to thermal equilibrium at longer annealing times. These diffusion reactions, together with kinetic equations to describe the time evolutions of {311} Si self-interstitial clusters and of EOR defects, lead to the following set of coupled partial differential equations:

$$\frac{\sigma C_{^{30}\mathrm{Si_S}}}{\sigma t} = G_I + G_V, \tag{4}$$

$$\frac{\sigma C_I}{\sigma t} = \frac{\sigma}{\sigma x}\left(D_I \frac{\sigma C_I}{\sigma x}\right) + G_I - G_{311} - G_{\mathrm{EOR}} + G_{\mathrm{Re}}, \tag{5}$$

$$\frac{\sigma C_{^{30}I}}{\sigma t} = \frac{\sigma}{\sigma x}\left(D_{^{30}I} \frac{\sigma C_{^{30}I}}{\sigma x}\right) - G_I, \tag{6}$$

$$\frac{\sigma C_V}{\sigma t} = \frac{\sigma}{\sigma x}\left(D_V \frac{\sigma C_V}{\sigma x}\right) + G_V + G_{\mathrm{Re}}, \tag{7}$$

$$\frac{\sigma C_{^{30}V}}{\sigma t} = \frac{\sigma}{\sigma x}\left(D_{^{30}V} \frac{\sigma C_{^{30}V}}{\sigma x}\right) - G_V, \tag{8}$$

$$\frac{\sigma C_{311}}{\sigma t} = G_{311}, \tag{9}$$

$$\frac{\sigma C_{\mathrm{EOR}}}{\sigma t} = 0, \tag{10}$$

where C_X is the concentration of X [$X = {}^{30}\mathrm{Si_S}$, I, ^{30}I, V, ^{30}V, I bound in {311} clusters ($X = 311$), I bound in EOR defect ($X = \mathrm{EOR}$)] and D_X is the diffusivity of X [$X = I, {}^{30}I, V, {}^{30}V$]. ^{30}Si atoms in {311} clusters and EOR defects are not taken into account because I's in {311} clusters and EOR defects are from the matrix and the matrix is composed predominantly by ^{28}Si. The total number of Si self-interstitials stored in EOR defects remains constant during annealing due to Ostwald ripening, as has been reported in Ref. 1. This result indicates that the amount of Si self-interstitials from EOR defects as a source of TED is much smaller than the total number of Si self-interstitials stored in EOR defects (C_{EOR}), and hence, the change in C_{EOR} with time can be neglected. Therefore, C_{EOR} is assumed to be time independent, which is represented by Eq. (10). G_x and G_{Re} denote the following generation terms:

$$G_I = k_{I\mathrm{f}} C_{^{30}I} - k_{I\mathrm{b}} C_{^{30}\mathrm{Si_S}} C_I, \tag{11}$$

$$G_V = k_{V\mathrm{f}} C_{^{30}V} - k_{V\mathrm{b}} C_{^{30}\mathrm{Si_S}} C_V, \tag{12}$$

$$G_{\mathrm{Re}} = k_{\mathrm{Re}}(C_I^{\mathrm{eq}} C_V^{\mathrm{eq}} - C_I C_V), \tag{13}$$

$$G_{311} = k_{311} C_{311}(C_I - C_I^{311}), \tag{14}$$

$$G_{\mathrm{EOR}} = k_{\mathrm{EOR}} C_{\mathrm{EOR}}(C_I - C_I^{\mathrm{EOR}}), \tag{15}$$

where G_I, G_V, and G_{Re} denote reactions (1), (2), and (3), respectively. k_I and k_V are the reaction rate constants of interstitial and vacancy mechanisms for Si self-diffusion with f and b denoting forward and backward, and k_{Re} is the g-r rate. The superscript eq denotes thermal equilibrium values. The contributions of ^{30}V and ^{30}V to ^{30}Si diffusion, $D^{\mathrm{eff}}_{^{30}I}$ and $D^{\mathrm{eff}}_{^{30}V}$, respectively, can be described by the following formulas in analogy with effective dopant diffusivities:

$$D^{\mathrm{eff}}_{^{30}I} = \frac{D_{^{30}I} C^{\mathrm{eq}}_{^{30}I}}{C_{^{30}\mathrm{Si_S}}}, \tag{16}$$

$$D^{\mathrm{eff}}_{^{30}V} = \frac{D_{^{30}V} C^{\mathrm{eq}}_{^{30}V}}{C_{^{30}\mathrm{Si_S}}}. \tag{17}$$

[This article is copyrighted as indicated in the article. Reuse of AIP content is subject to the terms at: http://scitation.aip.org/termsconditions. Downloaded to] IP: 131.113.64.57 On: Tue, 06 Oct 2015 08:51:35

For the values of $D^{\rm eff}_{^{30}I}$ and $D^{\rm eff}_{^{30}V}$, the contributions of I and V mechanisms to Si self-diffusion,[20] $f_I D_I C_I^{eq}/C_0$ and $f_V D_V C_V^{eq}/C_0$, respectively, were used. Here, f_I and f_V are the correlation factors for I and V mechanisms of Si self-diffusion, respectively, and C_0 is the concentration of the Si atoms. The values of $f_I = 0.73$ (Ref. 27) and $f_V = 0.5$ (Ref. 28) for the diamond structure were used in the same way as in our previous study.[20] Then, solving Eqs. (4)–(10) leads to Si self-diffusion under non-equilibrium conditions with the Si self-diffusivity described by

$$D^{\rm SD}_{\rm Si} = \frac{D_{^{30}I} C_{^{30}I}}{C_{^{30}{\rm Si}_s}} + \frac{D_{^{30}V} C_{^{30}V}}{C_{^{30}{\rm Si}_s}} = f_I \frac{D_I C_I}{C_0} + f_V \frac{D_V C_V}{C_0}. \quad (18)$$

For Eqs. (14) and (15), G_{311} and G_{EOR} represent the time evolutions of {311} clusters and EOR defects, respectively, and C_I^{311} and $C_I^{\rm EOR}$ denote the I concentrations maintained by {311} clusters and EOR defects. k_{311} and k_{EOR} are the time dependent rates for defect evolutions of {311} clusters and EOR defects. In order to fit the ^{30}Si profiles shown in Fig. 3, Eqs. (4)–(10) were solved numerically by the partial differential equation solver ZOMBIE[29] using the set of parameters described below. For the initial ^{30}Si profile, the profile measured after Ge implantation and shown in Fig. 1 has been used to take into account its perturbation due to Si displacement during the Ge implantation.

The evolution of {311} clusters consists of two time regimes: the evolution is initially governed by Ostwald ripening of {311} clusters and then by the dissolution of {311} clusters. The time dependence of k_{311} is described by the following equations:[30]

$$k_{311} = -at + b \quad (-at + b > k_{311{\rm b}}/C_I^{311}), \quad (19)$$

$$k_{311} = k_{311{\rm b}}/C_I^{311} \quad (-at + b \le k_{311{\rm b}}/C_I^{311}). \quad (20)$$

Here, a and b are constants, and t denotes annealing time. Equation (19) represents the {311} cluster growth rate, and Eq. (20) indicates the dissolution that is determined by the {311} cluster dissolution rate, $k_{311{\rm b}}$. The following values of essential parameters from Ref. 21 were used for the calculation: $C_I^{311} = 1.86 \times 10^{22} \exp(-1.80\,{\rm eV}/k_B{\rm T})\,{\rm cm}^{-3}$, $a = 2.55 \times 10^{-9} \exp(-1.71{\rm eV}/k_B{\rm T}){\rm cm}^3{\rm s}^{-2}$, $b = 1.15 \times 10^{-11} \exp(-0.83{\rm eV}/k_B{\rm T}){\rm cm}^3{\rm s}^{-1}$, and $k_{311{\rm b}} = 7.54 \times 10^{13} \exp(-3.51{\rm eV}/k_B{\rm T})\ {\rm s}^{-1}$. For the initial profile of C_{311}, a "+1" model[31] was used, where the implanted Ge profile beneath the a/c interface is multiplied by a factor of 1.0 [see Figs. 1 and 2(a)].[32] For EOR defects, $K_{\rm EOR} \equiv k_{\rm EOR} C_{\rm EOR}$, rather than the individual parameters $k_{\rm EOR}$ and $C_{\rm EOR}$, is an essential parameter to describe the evolution of EOR defects because $C_{\rm EOR}$ is assumed to be time independent due to Ostwald ripening.[1] The $C_{\rm EOR}$ profile is defined as a rectangular shape so that $K_{\rm EOR}$ has a non-zero constant value at the depth of 175–225 nm. Concerning Ostwald ripening of EOR defects, $C_I^{\rm EOR}$ is described as

$$\frac{C_I^{\rm EOR}}{C_I^{\rm eq}} = \exp\left(\frac{B}{r}\right), \quad (21)$$

$$r = \sqrt{Kt/2 + r_0{}^2}, \quad (22)$$

$$B = r_0 \times \ln\left[\frac{C_I^{\rm EOR}(t=0)}{C_I^{\rm eq}}\right], \quad (23)$$

using a mean radius of EOR defects r and a constant B that only depends on temperature.[8] Here, K is the ripening rate and r_0 is the initial mean radius. For the fitting, the values calculated by $K = 3.14 \times 10^7/T \exp(-4.53/k_B{\rm T})\ {\rm cm}^2\ {\rm s}^{-1}$ and $r_0 = 10$ nm from Ref. 1 were used, as we have done previously.[8] The values of $K_{\rm EOR}$ and $C_I^{\rm EOR}(t=0)/C_I^{\rm eq}$ are determined in this study from the fitting of ^{30}Si profiles in Fig. 3, except from those of the fifth ^{28}Si layer, where an additional enhanced diffusion was observed, as described above. Figure 4 shows these values as a function of temperature, and $K_{EOR} = 7.94 \times 10^{11} \exp(-1.74\,{\rm eV}/k_B{\rm T})\ {\rm s}^{-1}$ and $C_I^{\rm EOR}(t=0)/C_I^{\rm eq} = 1.34 \times 10^{-3} \exp(0.804\,{\rm eV}/k_B{\rm T})$ were obtained from Arrhenius fitting to the data. We stress that these two parameters deduced from the direct observation of Si self-diffusion are more reliable than the previous values determined from B diffusion because extraction of Si self-diffusion from the B diffusion profile can be affected by the formation of immobile B impurities as results of trapping by EOR defects[17] and/or precipitation.[33] The solid lines in Fig. 3 show the calculated profiles of ^{30}Si after annealing at (a) 800 °C, (b) 900 °C, and (c) 950 °C. The calculation results well reproduce the SIMS profiles; however, only the diffusion at the fifth ^{28}Si layer is obviously underestimated. This clearly indicates further enhancement of Si self-diffusion at the EOR defect region, in addition to the TED that has been extensively studied, as mentioned above.

B. Enhanced Si self-diffusion by tensile strain originated from EOR defects

In order to fit the ^{30}Si profiles that show the additional enhanced diffusion, we add an enhancement due to tensile strain induced by EOR defects to the TED model used

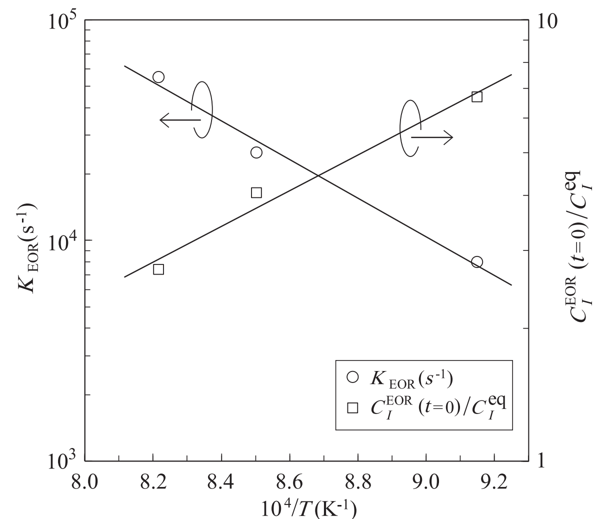

FIG. 4. Temperature dependence of the parameter values deduced from the calculation for $K_{\rm EOR}$ (open circles) and $C_I^{\rm EOR}(t=0)/C_I^{\rm eq}$ (open squares). Solid lines show Arrhenius fitting to the data.

[This article is copyrighted as indicated in the article. Reuse of AIP content is subject to the terms at: http://scitation.aip.org/termsconditions. Downloaded to] IP: 131.113.64.57 On: Tue, 06 Oct 2015 08:51:35

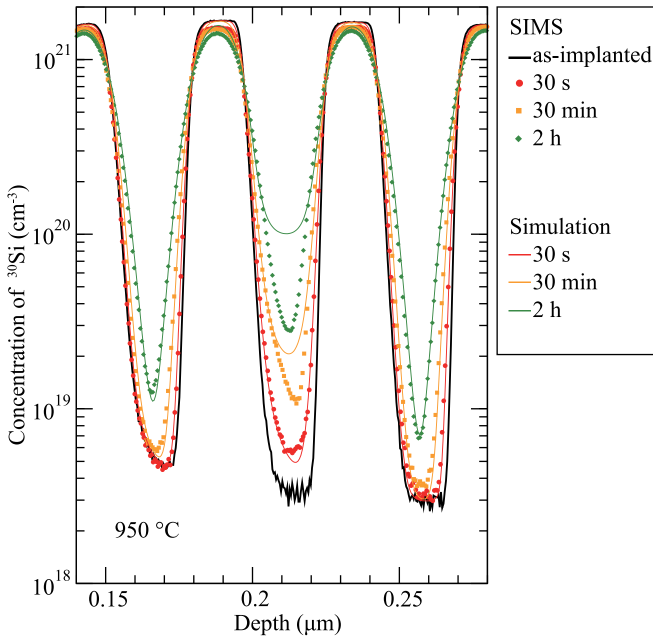

FIG. 5. SIMS and calculated profiles of ^{30}Si with 150 keV, 2×10^{15} cm^{-2} Ge implantation and annealing at 950 °C for 30 s, 30 min, and 2 h. Symbols and solid lines represent SIMS and calculated profiles, respectively. The SIMS profile before annealing (as-implanted) is also shown by a thick solid line. The calculation takes into account diffusion enhancement by tensile strain using a time independent value of f_{st} [see Eq. (25)]. The EOR defect region is enlarged.

above. Experimental results of X-ray analysis show the presence of tensile strain at EOR defect regions.[13–15] This tensile strain at EOR defects can enhance Si self-diffusion because theoretical calculations found that tensile strain enhances interstitial-mediated diffusion.[16] Therefore, it is reasonable to assume that I diffusion is enhanced by tensile strain at EOR defects because the Si self-diffusion observed in this study is mainly governed by I.

In order to take into account the enhanced I diffusion by local tensile strain at EOR defects, an enhancement factor F_{st} is introduced as follows:

$$D'_I = (F_{st} + 1)D_I, \tag{24}$$

$$F_{st} = f_{st} \exp\left(\frac{-(x - A_1)^2}{2A_2{}^2}\right), \tag{25}$$

where D'_I is the enhanced I diffusivity, which is substituted for D_I in Eq. (5). We assume that F_{st} has a Gaussian shape with the peak position A_1 and the width A_2. The ^{30}Si profiles were well reproduced when $A_1 = 211$ nm and $A_2 = 4.1$ nm were used, as will be described below. f_{st} is a strain enhancement factor, and the ^{30}Si profile at 950 °C for 30 s can be fitted using $f_{st} = 27$, as shown in Fig. 5, where the EOR defect region is enlarged. For longer annealing times, however, the calculation tends to overestimate the diffusion. This indicates that the enhancement of I diffusion due to strain decreases with time. The strain reduction with time is supported by X-ray measurement results that the strain induced by EOR defects decreases with higher annealing temperature.[14] A possible origin of the reduction of tensile strain with time is Ostwald ripening of EOR defects, during which they reduce their density and grow in size with time. Therefore, we assume that the strain reduction is correlated with the increase of mean radius of EOR defects and that f_{st} is described by the formula

$$f_{st} = f_0^{st} r_0{}^2/r^2, \tag{26}$$

where f_0^{st} is the f_{st} value at $t = 0$.

Figure 6 shows the calculated profiles of ^{30}Si near the EOR defect region. The calculation well reproduces all the SIMS profiles when the initial depth profile of F_{st} with $f_0^{st} = 27$ shown in Fig. 7 is used. Because the strain is applied only around the 210 nm region, the calculated results in other region are exactly the same as those in Fig. 3. It should be emphasized that the strain distribution indicated by F_{st} well coincides with the position of EOR defects, i.e., at the depth of 175–225 nm [Fig. 2(b)]. This result leads us to conclude that the additional enhanced Si self-diffusion is originated

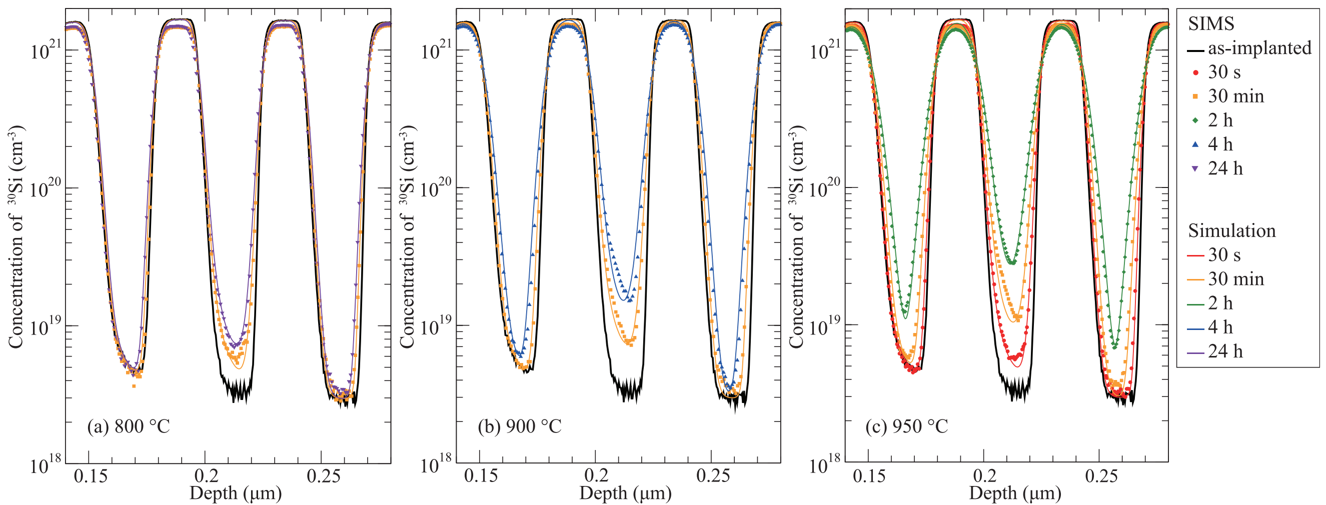

FIG. 6. SIMS and calculated profiles of ^{30}Si with 150 keV, 2×10^{15} cm^{-2} Ge implantation and annealing at (a) 800 °C for 30 min and 24 h, (b) 900 °C for 30 min and 4 h, and (c) 950 °C for 30 s, 30 min, and 2 h. Symbols and solid lines represent SIMS and calculated profiles, respectively. The SIMS profile before annealing (as-implanted) is also shown by a thick solid line. The calculation takes into account diffusion enhancement by tensile strain associated with Ostwald ripening of EOR defects [see Eq. (26)]. The EOR defect region is enlarged.

[This article is copyrighted as indicated in the article. Reuse of AIP content is subject to the terms at: http://scitation.aip.org/termsconditions. Downloaded to] IP: 131.113.64.57 On: Tue, 06 Oct 2015 08:51:35

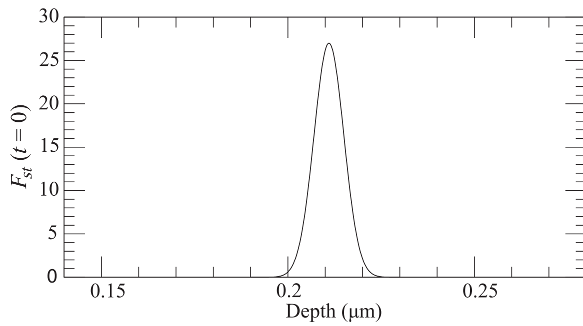

FIG. 7. Initial depth profile of F_{st} with $f_0^{st} = 27$ used in the calculation for Fig. 6.

from tensile strain induced by EOR defects and is associated with Ostwald ripening, in which the enhancement is inversely proportional to r^2. Figure 8 shows the decrease of f_{st} with time calculated by Eqs. (22) and (26), which is correlated with the increase of mean radius of EOR defects. The strain is reduced faster with longer annealing time and with higher temperature; however, f_{st} can be treated as a time independent parameter for annealing shorter than about 10 s below 950 °C, where the decrease of f_{st} is small enough.

The enhancement factor F_{st} obtained above is estimated in terms of the concept of an activation volume, by which the effect of strain on diffusion in solids can be thermodynamically treated.[34,35] The activation volume corresponds to the volume change of the system upon diffusion and the change in the activation enthalpy of diffusion with strain can be explained by the activation volume. The change in activation enthalpy of I diffusion Q' with tensile strain is estimated by Eq. (37) of Ref. 34

$$\frac{D_I'}{D_I} = \exp\left(\frac{-\varepsilon_{\mathrm{EOR}} Q'}{kT}\right), \tag{27}$$

where ε_{EOR} is the strain induced by EOR defects. The tensile strain induced by EOR defects is estimated to be about 1×10^{-2} from X-ray analysis.[13–15] Using $D_I'(t=0)/D_I = 28$ from the present study and $\varepsilon_{EOR} = 1 \times 10^{-2}$ leads to $Q' \approx -30$ eV per unit tensile strain from Eq. (27). This value is compatible with $Q' = -32 \pm 10$ eV per unit tensile strain obtained from B diffusion in Si under biaxial strain,[35] which is governed by the interstitial mechanism.[12] Therefore, the additional enhanced Si self-diffusion observed in the present study can be explained by tensile strain induced by EOR defects.

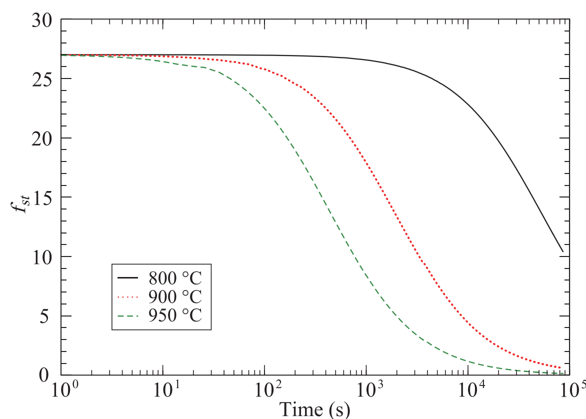

FIG. 8. Time dependence of f_{st} correlated with the increase of mean radius of EOR defects calculated by Eqs. (22) and (26). Solid, dotted, and dashed lines show the profiles of 800 °C, 900 °C, and 950 °C, respectively.

V. CONCLUSIONS

Si self-diffusion in the presence of EOR defects has been investigated using ^{nat}Si/^{28}Si isotope multilayers that are amorphized by Ge implantation. The behavior of Si self-interstitials is directly observed through ^{30}Si diffusion without any disturbance from dopant trapping at EOR defects. We have found further enhancement of Si self-diffusion at the EOR defect region in all annealing conditions, in addition to the TED. To explain this additional enhanced diffusion, an enhancement of I diffusion due to local tensile strain induced by EOR defects was introduced to the TED model. The enhancement is associated with Ostwald ripening of EOR defects and is inversely proportional to the square of mean radius. The diffusion calculation based on this model has well reproduced all the experimental ^{30}Si profiles. In addition, the enhancement of I diffusion deduced from the present study is compatible with that of B diffusion in terms of the concept of an activation volume. The present results will be helpful for a comprehensive understanding of defect-induced strain and its effect on diffusion.

ACKNOWLEDGMENTS

This work was supported in part by the Grant-in-Aid for Scientific Research by MEXT, NanoQuine, JSPS Core-to-Core Program, Cooperative Research Project Program of the RIEC, Tohoku University, and Grants-in-Aid for Scientific Research No. 24560413 from JSPS.

[1] C. Bonafos, D. Mathiot, and A. Claverie, J. Appl. Phys. **83**, 3008 (1998).
[2] A. Al-Bayati, S. Tandon, A. Mayur, M. Foad, D. Wagner, R. Murto, D. Sing, C. Ferguson, and L. Larson, in *IEEE Proc. Conf. Ion Implantation Tech.* (2000), p. 54.
[3] D. K. Sadana, W. Maszara, J. J. Wortmann, G. A. Rozgonyi, and W. K. Chu, J. Electrochem. Soc. **131**, 943 (1984).
[4] H. S. Chao, P. B. Griffin, and J. D. Plummer, Appl. Phys. Lett. **68**, 3570 (1996).
[5] K. S. Jones, S. Prussin, and E. R. Weber, Appl. Phys. A **45**, 1 (1988).
[6] A. Claverie, B. Colombeau, G. Ben Assayag, C. Bonafos, F. Cristiano, M. Omri, and B. de Mauduit, Mater. Sci. Semicond. Process. **3**, 269 (2000).
[7] N. E. B. Cowern, D. Alquier, M. Omri, A. Claverie, and A. Nejim, Nucl. Instrum. Methods Phys. Res., Sect. B **148**, 257 (1999).
[8] M. Uematsu, Jpn. J. Appl. Phys., Part 2 **38**, L1213 (1999).
[9] E. Lampin, V. Senez, and A. Claverie, J. Appl. Phys. **85**, 8137 (1999).
[10] N. E. B. Cowern, K. T. F. Janssen, and H. F. F. Jos, J. Appl. Phys. **68**, 6191 (1990).
[11] K. S. Jones, L. H. Zhang, V. Krishnamoorthy, M. Law, D. S. Simmons, P. Chi, L. Rubin, and R. G. Elliman, Appl. Phys. Lett. **68**, 2672 (1996).
[12] P. M. Fahey, P. B. Griffin, and J. D. Plummer, Rev. Mod. Phys. **61**, 289 (1989).
[13] P. Zaumseil, U. Winter, F. Cembali, M. Servidori, and Z. Sourek, Phys. Status Solidi A **100**, 95 (1987).
[14] A. Pesek, Appl. Phys. A **58**, 141 (1994).
[15] S. Solmi, F. Cembali, R. Fabbri, M. Servidori, and R. Canteri, Appl. Phys. A **48**, 255 (1989).
[16] O. Sugino and A. Oshiyama, Phys. Rev. B **46**, 12335 (1992).

[This article is copyrighted as indicated in the article. Reuse of AIP content is subject to the terms at: http://scitation.aip.org/termsconditions. Downloaded to] IP: 131.113.64.57 On: Tue, 06 Oct 2015 08:51:35

[17]E. M. Bazizi, P. F. Fazzini, C. Zechner, A. Tsibizov, H. Kheyrandish, A. Pakfar, L. Ciampolini, C. Tavernier, and F. Cristiano, Mater. Sci. Eng., B **154–155**, 275 (2008).
[18]T. Noda, J. Appl. Phys. **91**, 639 (2002).
[19]R. Kim, T. Hirose, T. Shano, H. Tsuji, and K. Taniguchi, Jpn. J. Appl. Phys., Part 1 **41**, 227 (2002).
[20]Y. Shimizu, M. Uematsu, and K. M. Itoh, Phys. Rev. Lett. **98**, 095901 (2007).
[21]Y. Shimizu, M. Uematsu, K. M. Itoh, A. Takano, K. Sawano, and Y. Shiraki, J. Appl. Phys. **105**, 013504 (2009).
[22]H. Bracht, Phys. Rev. B **75**, 035210 (2007).
[23]H. Bracht, H. Silvestri, I. Sharp, and E. Haller, Phys. Rev. B **75**, 035211 (2007).
[24]T. Kojima, R. Nebashi, K. M. Itoh, and Y. Shiraki, Appl. Phys. Lett. **83**, 2318 (2003).
[25]Y. Shimizu, M. Uematsu, K. M. Itoh, A. Takano, K. Sawano, and Y. Shiraki, Appl. Phys. Express **1**, 021401 (2008).
[26]M. Naganawa, Y. Shimizu, M. Uematsu, K. M. Itoh, K. Sawano, Y. Shiraki, and E. E. Haller, Appl. Phys. Lett. **93**, 191905 (2008).
[27]K. Compaan and Y. Haven, Trans. Faraday Soc. **54**, 1498 (1958).
[28]K. Compaan and Y. Haven, Trans. Faraday Soc. **52**, 786 (1956).
[29]W. Jüngling, P. Pichler, S. Selberherr, E. Guerrero, and H. W. Pötzl, IEEE Trans. Electron Devices **32**, 156 (1985).
[30]M. Uematsu, Jpn. J. Appl. Phys., Part 2 **36**, L982 (1997).
[31]M. D. Giles, J. Electrochem. Soc. **138**, 1160 (1991).
[32]H. S. Chao, S. W. Crowder, P. B. Griffin, and J. D. Plummer, J. Appl. Phys. **79**, 2352 (1996).
[33]S. Solmi, F. Baruffaldi, and R. Canteri, J. Appl. Phys. **69**, 2135 (1991).
[34]M. Aziz, Y. Zhao, H.-J. Gossmann, S. Mitha, S. Smith, and D. Schiferl, Phys. Rev. B **73**, 054101 (2006).
[35]N. R. Zangenberg, J. Fage-Pedersen, J. L. Hansen, and A. N. Larsen, J. Appl. Phys. **94**, 3883 (2003).

[This article is copyrighted as indicated in the article. Reuse of AIP content is subject to the terms at: http://scitation.aip.org/termsconditions. Downloaded to] IP: 131.113.64.57 On: Tue, 06 Oct 2015 08:51:35